Radiomics Analysis for Evaluation of Pathological Complete Response to Neoadjuvant Chemoradiotherapy in Locally Advanced Rectal Cancer

Zhenyu Liu[1,2,†], Xiao-Yan Zhang[2,†], Yan-Jie Shi[2,†], Lin Wang[3], Hai-Tao Zhu[2], Zhenchao Tang[1], Shuo Wang[1], Xiao-Ting Li[2], Jie Tian[1,4,*], Ying-Shi Sun[2,*]

[1]CAS Key Laboratory of Molecular Imaging, Institute of Automation, Beijing, 100190, China

[2]Key laboratory of Carcinogenesis and Translational Research (Ministry of Education/Beijing), Department of Radiology, Peking University Cancer Hospital & Institute, Hai Dian District, Beijing, 100142, China.

[3]Key laboratory of Carcinogenesis and Translational Research (Ministry of Education/Beijing), Department of Gastrointestinal Surgery, Peking University Cancer Hospital & Institute, Hai Dian District, Beijing 100142, China.

[4]University of Chinese Academy of Sciences, Beijing, 100080, China

Running Title: Evaluation of *pCR* to NAC for rectal cancer via radiomics

[*]**Corresponding Author:**

Ying-Shi Sun

Telephone number: 86-10-88196822

Fax: 86-10-88196822

E-mail: sys27@163.com

Jie Tian

Telephone number: 86-10-82618465

Fax: 86-10-62527995

E-mail: jie.tian@ia.ac.cn

[†] **Zhenyu Liu, Xiao-Yan Zhang and Yan-Jie Shi contributed equally to this work**

AUTHOR CONTRIBUTIONS

Conception and design: Ying-Shi Sun, Jie Tian

Collection and assembly of data: Xiao-Yan Zhang, Yan-Jie Shi, Lin Wang

Development of methodology: Ying-Shi Sun, Shuo Wang, Xiao-Yan Zhang, Zhenchao Tang, Zhenyu Liu, Yan-Jie Shi, Hai-Tao Zhu, Xiao-Ting Li

Data analysis and interpretation: Zhenyu Liu, Xiao-Yan Zhang, Yan-Jie Shi, Shuo Wang, Zhenchao Tang, Hai-Tao Zhu, Xiao-Ting Li, Ying-Shi Sun, Jie Tian

Manuscript writing: All authors

Final approval of manuscript: All authors

Grant Support:

This work was supported by the National Natural Science Foundation of China (Grant No. 81471640, 81501549, 81227901, 81501621 and 61231004), the Key Research Program of the Chinese Academy of Sciences (Grant No. KGZD-EW-T03), the Science and Technology Service Network Initiative of the Chinese Academy of Sciences (Grant No.KFJ-SW-STS-160) and the Beijing Municipal Science & Technology Commission 'Capital Clinical Research Special Fund' (No.Z171100001017102, Z151100004015105).

Abstract

Purpose: To develop and validate a radiomics model for evaluating pathological complete response (*pCR*) to neoadjuvant chemoradiotherapy in patients with locally advanced rectal cancer (LARC).

Experimental Design: We enrolled 222 patients (152 in the primary cohort and 70 in the validation cohort) with clinicopathologically confirmed LARC who received chemoradiotherapy before surgery. All patients underwent T2-weighted and diffusion-weighted imaging before and after chemoradiotherapy; 2252 radiomic features were extracted from each patient pre- and post-treatment imaging. The 2-sample *t*-test and the least absolute shrinkage and selection operator regression were used for feature selection, whereupon a radiomics signature was built with support vector machines. Multivariable logistic regression analysis was then used to develop a radiomics model incorporating the radiomics signature and independent clinicopathological risk factors. The performance of the radiomics model was assessed by its calibration, discrimination, and clinical usefulness with independent validation.

Results: The radiomics signature comprised 30 selected features and showed good discrimination performance in both the primary and validation cohorts. The individualized radiomics model, which incorporated the radiomics signature and tumor length, also showed good discrimination, with an area under the receiver operating characteristic curve of 0.9756 (95% confidence interval: 0.9185–0.9711) in the validation cohort, and good calibration. Decision curve analysis confirmed the clinical utility of the radiomics model.

Conclusion: Using pre- and post-treatment MRI data, we developed a radiomics model with excellent performance for individualized, non-invasive prediction of *pCR*. This model may be used to identify LARC patients who can omit surgery after chemoradiotherapy.

Key words: locally advanced rectal cancer (LARC), radiomics, pathological complete response (*pCR*), diffusion-weighted MRI, T2-weighted MRI

Statement of translational relevance

In the present study, we developed and validated a radiomics model for noninvasive, individualized evaluation of pathological complete response (*pCR*) in patients with locally advanced rectal cancer (LARC) based on pre- and post-treatment MRI data. The model's validation data showed it to be robust in its ability to detect *pCR*. In addition to improved *pCR* detection, the model (and the derived nomogram that incorporates the radiomics signature and independent clinicopathologic risk factors) provides patients and doctors with an effective tool for evaluating chemoradiotherapeutic outcomes in patients with LARC and for determining further treatment plans.

Introduction

More than 100,000 people worldwide are diagnosed with rectal cancer annually; 70% are locally advanced rectal cancers (LARC). The current standard treatment for LARC is neoadjuvant chemoradiotherapy followed by total mesorectal excision (TME) (1-3). Approximately 15–27% of patients will show pathological complete response (*pCR*) to chemoradiotherapy (4,5), which led some investigators to question the use of TME in patients who achieve *pCR*. Several previous studies suggested that such patients usually have excellent long-term outcomes without surgery (6-9), and that the "wait and see" management approach that avoids surgery and preserves organs is a valid option (10). However, *pCR* can only be confirmed by histopathological examination of surgically resected specimens, and creating a noninvasive, validated method to safely and accurately identify *pCR* patients after chemoradiotherapy remains a major challenge.

Medical imaging can noninvasively evaluate the therapeutic responses to chemoradiotherapy. Several investigators have proposed methods to identify good responders to chemoradiotherapy using various pre- or post-treatment imaging data including fludeoxyglucose positron emission tomography (11), T2-weighted MRI (T2WI) (12), dynamic contrast-enhanced MRI (13), and diffusion-weighted imaging (DWI) (14,15). Although these imaging methods have the potential to predict or evaluate responses to chemoradiotherapy, their accuracy in evaluating *pCR* is limited. In a recent small-sample study, radiomics analysis based on pre-treatment multi-parametric MRI performed well in predicting *pCR* after chemoradiotherapy, albeit without independent validation (16). These results suggested that pre-treatment multi-parametric MRI may be associated with response to chemoradiotherapy, and that radiomics analysis may greatly contribute to determining whether pCR has been achieved after chemoradiotherapy.

Radiomics, which is based on advanced pattern recognition tools, involves the extraction of a large number of quantitative features from digital images to determine relationships between such features and the underlying pathophysiology (17,18). Radiomics analysis of large imaging datasets has been successfully employed in the field of oncology for noninvasively profiling tumor heterogeneity (19), and there is a growing interest within the field in devising maps that display the associations between tumor heterogeneity and imaging features (20). Recent advances in radiomics have enabled oncologists to deliver more personalized medical care that takes into account phenotypic subtypes (21), as well as to assess therapeutic responses using post-treatment imaging features (22,23). A recent radiomics study in patients with colorectal cancer proposed a nomogram to predict lymph node metastasis (24); this further confirmed the clinical value of radiomics. To that end, a radiomics

model for *pCR* detection could vastly improve treatment strategy planning. As pre-treatment MRI is associated with responses to chemoradiotherapy while post-treatment MRI directly reflects the post-treatment status, a radiomics model combining pre- and post-treatment MRI data may potentially predict *pCR* with accuracy.

In the present study, we aimed to develop and validate a radiomics model for individualized *pCR* evaluation after chemoradiotherapy in patients with LARC. Consistent with clinical practice, our work combined pre- and post-treatment MRI data to non-invasively evaluate the outcomes of such patients and to select LARC patients for whom surgery can be avoided.

Materials and Methods

Patients

This retrospective study was approved by the ethics committee of Beijing Cancer Hospital; the informed consent requirement was waived. All procedures performed in studies involving human participants were in accordance with the 1964 Helsinki declaration and its later amendments. A total of 222 patients who underwent surgical treatment between July 2010 and June 2015 were consecutively included in this study according to the following inclusion and exclusion criteria (Figure S1). The inclusion criteria were (i) biopsy-proven primary rectal adenocarcinoma; (ii) locally advanced disease determined by pre-treatment MRI (≥T3, and/or positive nodal status); (iii) received complete neoadjuvant chemoradiotherapy and no treatment has been done before; (iv) TME surgery was performed after completion of neoadjuvant chemoradiotherapy, after which *pCR* was confirmed by postoperative pathological examination; and (v) pre- and post-treatment MRI data obtained using the same 3-T MR scanner, including DWI and high-resolution T2WI. The exclusion criteria were (i) not completing neoadjuvant chemoradiotherapy; (ii) not undergoing surgery at our hospital, or *pCR* was not assessed; (iii) lack of DWI or high-resolution T2WI data; (iv) insufficient MRI quality to obtain measurements (e.g., owing to motion artifacts); (v) mucinous adenocarcinoma detected on pathological examination after TME; and (vi) lack of pre-surgical carcinoembryonic antigen (CEA) and CA19-9 data. Patients were allocated to primary and validation cohorts according to the time of surgery in a 2:1 ratio; the first 152 patients were allocated to the primary cohort and the subsequent 70 were allocated to the validation cohort. The clinical characteristics of all patients are shown in Table 1; the data analysis flowchart of the study is shown in Figure 1.

Neoadjuvant Chemoradiotherapy Treatment

All patients received preoperative chemoradiotherapy followed by TME. Intensity-modulated radiation therapy (IMRT) was administered using a Varian Rapidarc system (Varian Medical Systems, USA). The IMRT regimen comprised 22 fractions of 2.3 Gy (gross tumor volume, GtV) and 1.9 Gy (clinical target volume, CtV). A total dose of 50.6 Gy (GtV)/41.8 Gy (CtV) was administered 5 times per week over a period of 30 days (25,26). The GtV was defined as the volume of the primary tumor including the mesorectum. The CtV was defined as the primary tumor, mesorectal region, presacral region, mesorectal lymph nodes, lateral lymph nodes, internal iliac lymph node chain, and pelvic wall area. Capecitabine treatment was administered concurrently with IMRT at a dose of 825 mg/m^2 orally twice per day. TME-based surgery was recommended 8 weeks after completing chemoradiotherapy. Adjuvant chemotherapy was routinely recommended; capecitabine alone, mFOLFOX6, or CapeOx were prescribed at the discretion of the physician.

Pathological Assessment of Response

Surgically resected specimens were histopathologically examined and analyzed by an experienced pathologist and were further reviewed by a dedicated gastrointestinal pathologist, both of whom were blinded to the MRI data; *pCR* was defined as the absence of viable tumor cells in the primary tumor and lymph nodes.

MRI Data Acquisition and Retrieval Procedure

All patients underwent MRIs at 2 time points: Within 1 week before the initiation of neoadjuvant chemoradiotherapy and within 1 week before surgery (defined as pre- and post-treatment MRI, respectively). All MRIs were performed with a 3.0-T MR scanner (Discovery 750; GE Healthcare) using an 8-channel phased array body coil in the supine position. To reduce colonic motility, 20 mg of scopolamine butylbromide was injected intramuscularly 30 min prior to MRI scanning. Patients were not required to undergo bowel preparation before the examination. All patients underwent a conventional rectal MRI protocol including DWI and axial, coronal, and sagittal T2-weighted images. DWI images were obtained using single-shot echo-planar imaging with 2 b-factors (0 and 1000 s/mm^2), and repetition time (TR) = 2800 ms, echo time (TE) = 70 ms, field of view (FOV) = 340 × 340 mm, matrix = 256×256, thickness = 4.0 mm, and gap = 1.0 mm. Apparent diffusion coefficient (ADC) maps were generated automatically and included both b values in a monoexponential decay model. High resolution T2WI images were obtained using fast recovery fast spin echo with TR = 5694 ms, TE = 110 ms, FOV = 180×180 mm, echo train length = 24, matrix = 288×256, thickness =

3.0 mm and gap = 0.3 mm.

All MRI scans were retrieved from the picture archiving and communication system for further image feature extraction.

Tumor Masking

Pre- and post-treatment MRIs were analyzed by 2 radiologists (Dr. Zhang, a radiologist with 10 years of experience in rectal cancer imaging, and Dr. Shi, who has 7 years of experience in rectal cancer imaging); both were blinded to the histopathology results. The regions of interest (ROIs) were created manually via the itk-SNAP software (www.itksnap.org) using the T2WI and DWI data, including the whole tumor and excluding the intestinal lumen. ROIs of rectal tumors before and after therapy were manually drawn on each slice. Before chemoradiotherapy, ROIs were drawn along the contour of the tumor as visualized by T2WI (slightly high signal), containing the surrounding chords and burrs. ROIs were placed on the high signal intensity region on DWI (b-value of 1000 s/mm^2) on each slice. If a highly suspicious tumor signal was still noted on T2WI (slightly high signal) after chemoradiotherapy, the ROI delineating criteria were the same as those before chemoradiotherapy. If a low, mixed-intensity, or any other non-normal rectal wall signal was detected in the tumor bed on T2WI (abnormal signal), the ROIs were drawn with contouring of the abnormal signal region. In cases where no abnormal signals were detected on T2WI (iso-intensity signal compared with the normal rectal wall), the ROIs were placed on the primary tumor bed region determined by T2WI before chemoradiotherapy. Due to the higher resolution of DWI compared to ADC maps, ROIs were detected with a b-value of 1000 s/mm^2 first and then copied to the corresponding ADC maps. If a highly suspicious tumor signal (high signal) was noted on DWI, the ROIs were placed over the high-signal region. In cases where no high signal was detected on DWI compared to the normal rectal wall, the ROIs were placed on the primary tumor bed region as determined by DWI before chemoradiotherapy. Care was taken to avoid the magnetic susceptibility artifact during DWI. If no tumor signals were noted on post-chemoradiotherapy T2WI, then the ROI of DWI was outlined on the corresponding tumor bed region based on pre-treatment images.

Radiomic Feature Extraction and Statistical Analysis

MRI scans for each patient were normalized with z-scores in order to obtain a standard normal distribution of image intensities. Next, 3 groups of imaging features were extracted from the normalized pre- and post-treatment T2WI and DWI data with manually segmented ROIs: (i) 4 statistical features, (ii) 43 voxel-intensity computational features, and (iii) 516 wavelet features.

Group 1 consisted of quantified tumor intensity characteristics with first-order statistics calculated from the histogram of all tumor intensities. Group 2 comprised textual features based on the quantification of intratumoral heterogeneity (i.e., differences in texture observed within the tumor volume); these features were all calculated using 2-dimensional analysis and averaged for all slices within the 3-dimensional tumor volume. Group 3 incorporated the calculated textural features from the wavelet decompositions of the original images, thereby focusing on the various frequency scales and different feature orientations within the tumor volume. All of these features have generally been used in previous radiomics studies (19,21,24). The final set comprised of 563 features for each modality (T2WI and DWI) per MRI scan, resulting in a total of 2252 radiomic features per patient. All feature-extracting algorithms were implemented using the Matlab software (Math Works Inc., Natick, MA); details are provided in the supporting information. Additionally, all statistical analyses were conducted with MatlabR2014b (Math Works Inc.). The reported statistical significance levels are all 2-sided, with the statistical significance set at 0.05.

Inter- and Intra-observer Reproducibility Evaluation

Inter-observer and intra-observer reproducibility of ROI detection and radiomic feature extraction were initially determined using the T2WI data of 80 consecutive patients undergoing investigation between July 2010 and May 2011 for ROI-based radiomic feature generation in a blinded fashion by Dr. Zhang and Dr. Shi. To assess intra-observer reproducibility, each reader repeated the generation of radiomic features twice within a 1-week period following the same procedure. Intra-class correlation coefficients were used to evaluate the intra- and inter-observer agreement in terms of feature extraction; we interpreted a coefficient of 0.81–1.00 as almost perfect agreement, 0.61–0.80 as substantial agreement, 0.41–0.60 as moderate agreement, 0.21–0.40 as fair agreement, and 0–0.20 as poor or no agreement (27). Many radiomic features described the shape and size of the ROIs; therefore, these values could also be used to evaluate the overall inter- and intra-observer reproducibility of the ROIs.

Feature Selection Method

To reduce over-fitting or any type of bias in our radiomics model, 2 feature selection steps were used. First, the best features based on univariate statistical tests (2-sample *t*-test) between *pCR* and non-*pCR* groups in the primary cohort were selected. Second, regularized multivariate logistic regression with the least absolute shrinkage and selection operator (LASSO) penalty was applied to the data of the primary cohort. With a linear combination of the selected features weighted by their respective coefficients, a model was used to estimate the chemoradiotherapy outcomes based on the

radiomic features. The model was defined as follows:

$$y = \sum_{j=1}^{d} \beta_j x_j + \beta_0 + \varepsilon$$

Where y is 1 for patients with *pCR* and 0 for non-*pCR* patients; d is the number of features used in the model; x_j ($j = 1, 2, \ldots, d$) is the feature; β_j ($j = 0, 1, 2, \ldots, d$) is the model parameter, and Ɛ is the error term.

Using regularized regression to estimate the parameters of the model, feature selection (by forcing many parameters to zero value) can be performed simultaneously. The aim of this approach is to minimize the cost function:

$$\sum_{i=1}^{N} \left[y_i - S\left(\sum_{j=1}^{d} \beta_j x_{ij} + \beta_0 \right) \right]^2 + \lambda \sum_{j=1}^{d} |\beta_j|$$

Where y_i is the outcome of patient i, N is the number of patients, S is the sigmoid function, x_{ij} is the jth feature of the ith patient, and λ is the regularization parameter. The sigmoid function S is defined as follows:

$$S(x) = \frac{1}{1 + e^{-x}}$$

with the LASSO penalty $\sum_{j=1}^{d} |\beta_j|$ applied, leading to sparse models by setting some parameters (β_j s) to zero. Features with greater contributions to the model are selected.

Radiomics Signature Construction

The support vector machine (SVM) method was used to discriminate whether a patient achieved *pCR* in this study. A radiomics score was calculated for each patient using an SVM model with linear kernel training based on the selected features. Leave-one-out cross-validation (LOOCV) was employed to determine the optimal value of the regularization parameter C using the primary cohort. The C value that maximized the area under the receiver operating characteristic curve (AUC) in the primary cohort was selected as the optimal regularization parameter. Specifically, we tested values of $C \in [0.01, 1]$ with a step size of 0.02. After C was selected, the radiomics score for each patient in the validation cohort was calculated using the SVM model. The AUC, classification accuracy, positive predictive value (PPV), and negative predictive value (NPV) were calculated as metrics to

assess the quantitative discrimination performance of the radiomics signature in both the primary and validation cohorts.

Development of the Individualized Radiomics Model

Multivariable logistic regression analysis was conducted with the following clinical information: age, sex, post-treatment CEA, post-treatment CA19-9, histological grade, pre- and post-treatment tumor length, pre- and post-treatment tumor thickness obtained from oblique axial T2WI (TTOA), pre- and post-treatment invasion distance beyond the muscularis propria (IDBMP), pre- and post-treatment shortest distance between the mesorectal fascia and the outer edge of the tumor extension (SDBMT), pre- and post-treatment total number of the lymph nodes detected by DWI (NLN), pre- and post-treatment minor axis length of the largest lymph node (MALLLN), and radiomics signature. Backward step-wise selection was applied using the likelihood ratio test with Akaike's information criterion employed as the stopping rule.

Based on the multivariable logistic analysis of the aforementioned clinical parameters in the primary cohort, a radiomics model for *pCR* detection was constructed with the selected variates to provide a quantitative tool for clinical use.

Apparent Performance and Validation of the Radiomics Model

Calibration curves accompanied by the Hosmer-Lemeshow test were plotted to assess the radiomics model; a significance test statistic implied that the model was not perfectly calibrated (29). Harrell's C-index, classification accuracy, PPV, and NPV were measured to quantify the model's discriminatory performance. The model was subjected to bootstrapping validation (1,000 bootstrapping resamples including feature selection, model construction, and performance estimation) to achieve a relatively corrected performance.

The performance of the radiomics model was then tested in the validation cohort. The multivariable logistic regression formula devised based on the primary cohort was applied to the patients in the validation cohort, and the total points were calculated for each. Logistic regression was then performed using the total points of each patient in the validation cohort; the performance of the model was derived using regression analysis.

Calibration curves were calculated to determine the agreement between the estimated probability of *pCR* and the actual outcomes (i.e., the *pCR* rate) in both the primary and validation cohorts. In the graph, the y-axis represents the actual rate of *pCR* while the x-axis represents the calculated probability of *pCR*. The diagonal blue line represents a perfect diagnosis by an ideal model and the

pink line represents the performance of the radiomics model; a fit that is closer to the diagonal blue line represents better performance. The calibration curve was drawn by plotting $\hat{P}$ on the x-axis and $P_c = [1+\exp-(\gamma_0 + \gamma_1 L)]^{-1}$ on the y-axis, where P_c is the actual probability, $L = \text{logit}(\hat{P})$, $\hat{P}$ is the diagnosed probability, γ_0 is the corrected intercept, and γ_1 is the slope estimate.

Clinical Use

Decision curve analysis was conducted to determine the clinical usefulness of the radiomics model by quantifying the net benefits at different threshold probabilities in the validation dataset (30).

Results

Clinical Characteristics

The clinical characteristics of the patients are summarized in Tables 1 and S1. There were no significant differences between the 2 cohorts in terms of *pCR* prevalence (17.11% and 17.14% in the primary and validation cohorts, respectively, p=0.567). There were no significant differences in other clinical characteristics between the primary and validation cohorts except for pre-treatment N stage and post-treatment tumor length (Table S1). Additionally, a few clinical characteristics were significantly different between the *pCR* and non-*pCR* groups (Table 1), including post-treatment T stage, post-treatment N stage, pre-treatment IDBMP, pre-treatment MALLLN, post-treatment TTOA, post-treatment IDBMP, and post-treatment SDBMT; all of these characteristics were included in the *pCR* evaluation model.

Feature Selection and Radiomics Signature Construction

Satisfactory inter- and intra-observer reproducibility of radiomic feature extraction was achieved (Supporting Information).

To devise the radiomics signature, we first performed univariate analysis (2-sample *t*-tests) using the primary cohort as a pre-filter. To avoid eliminating highly discriminative features on multivariate analysis rather than on univariate analysis, more features than those that showed significant differences between the 2 groups were included as compensation. All features were sorted in increasing order of p-values, and the top 676 features (30%) were included in the next step of the analysis with p<0.0987. Next, 676 features were reduced to 30 potential predictors by applying regularized regression to the primary cohort with the LASSO penalty using LOOCV via minimum criteria (Figure 2).

Next, an SVM model with a linear kernel was constructed using the selected features based on the primary cohort. The best regularization parameter (C = 0.05) was determined by LOOCV. The resultant coefficients of the features used in calculating the radiomics score are shown in Table S2. The distributions of the radiomics scores and outcomes of chemoradiotherapy for each patient in the primary and validation cohorts are shown in Figure 3.

Diagnostic Validation of the Radiomics Signature

There was a significant difference in radiomics scores between *pCR* and *non-pCR* patients in the primary cohort ($p<0.01$); the same was true in the validation cohort ($p<0.01$). The radiomics signature yielded an AUC of 0.9744 (95% confidence interval [CI], 0.9642–0.9756) and a classification accuracy of 94.08% (95% CI, 93.19–94.79%) in the primary cohort, and an AUC of 0.9799 (95% CI, 0.9780–0.9840) and a classification accuracy of 94.29% (95% CI, 94.21–95.61%) in the validation cohort. More importantly, the radiomics signature achieved a PPV of 86.96% (95% CI, 84.84–90.40%) in the primary cohort and 90.00% (95% CI, 89.60–99.40%) in the validation cohort. Detailed information on radiomics signature performance is shown in Table 2.

Development, Performance, and Validation of the Individualized Radiomics Nomogram

The radiomics signature and post-treatment tumor length were identified as independent factors predicting *pCR* (Tables S3 and S4). The model that incorporated these independent predictors was developed and presented as a nomogram (Figure 4).

The calibration curve of the radiomics model estimating the probability of *pCR* demonstrated good agreement in the primary cohort (Figure 4). The Hosmer-Lemeshow test yielded a non-significant statistic ($p = 0.9609$), suggesting no departure from the perfect fit. The C-index for the radiomics model was 0.9799 (95% CI: 0.9517–1) within the primary cohort.

Good performance was also observed for the probability of *pCR* in the validation cohort (Figure 4). The Hosmer-Lemeshow test yielded non-significant statistics for the radiomics model ($p=0.5416$). The radiomics model also achieved good discrimination performance with a C-index of 0.9756 (95% CI: 0.9417–1) and classification accuracy of 94.29% (95% CI: 91.85–97.11%).

Clinical Use

The decision curve analysis result for the radiomics model is shown in Figure 4. The decision curve showed relatively good performance for the model in terms of clinical application. While the

probability of achieving *pCR* ranges from 0 to 100%, using the proposed radiomics model to detect *pCR* shows a greater advantage than either the scheme in which all patients are assumed to achieve *pCR* or the scheme in which no patients are.

Discussion

In the present study, we developed and validated a radiomics model that incorporated pre- and post-treatment MRI data for noninvasive, individualized prediction of *pCR* in patients with LARC. The easy-to-use nomogram facilitated noninvasive estimation of *pCR*. The proposed radiomics model performs well and thereby provides an effective tool for clinical decision-making.

The accurate detection of *pCR* using visual judgment (conventional MRI) remains challenging in clinical settings. Methods using multi-modality MRI (e.g. combining DWI and conventional MRI) (14,28-30) or positron emission tomography/CT (31) may also perform well; however, their levels of accuracy are not clinically reliable. Radiomics analysis integrates many high-dimensional imaging features used to evaluate *pCR* that are difficult to detect visually. Our proposed radiomics model based on these imaging features performed better than previously reported methods, and can therefore be useful in clinical decision-making as it provides radiologists and oncologists with a potential quantitative tool for individualized *pCR* prediction.

To use our proposed radiomics model, radiologists must first delineate the ROI on pre- and post-treatment MRI scans (T2WI and DWI), after which the model allows for the calculation of the probability of *pCR* for each individual patient. Oncologists can then consider various factors, including the calculated probability of *pCR* and other retrievable clinical information, as well as their own clinical experience and the patient's opinion, to make a comprehensive judgment on whether a wait-and-see treatment approach is warranted.

The radiomics model combined pre- and post-treatment T2WI and DWI data of patients with LARC, and demonstrated adequate discrimination in both the primary and validation cohorts. There were significant differences in pre-treatment N stage and post-treatment tumor length between these 2 cohorts. Nonetheless, the proposed radiomics model still performed appropriately and was well-calibrated. The results suggest that the radiomics model is robust in its evaluation of *pCR* and can be used in the clinical setting. Two recent studies investigated the *pCR* prediction capability of texture or radiomic features with DWI and multi-parametric MRI without independent validation; they derived AUCs less than 0.9 (15,16), which was a much lower value than the independent validation results obtained in our study. Specifically, our proposed radiomics model achieved a relatively high NPV and PPV in both the primary and validation cohorts. The high NPV indicated

that the *non-pCR* evaluation of the proposed model was reliable. Thus, surgeons may potentially forgo colonoscopies or other examinations meant to confirm the absence of residual lesions in *non-pCR* patients, and can thereby avoid excessive treatments that would ensue in the event that a *pCR* patient is incorrectly judged to be a *non-pCR* patient. Conversely, the high PPV suggests that our model can satisfactorily enable surgeons to screen out *pCR* patients, allowing for a "watch and wait" approach. Patients who were designated *pCR* using our model had a relatively high probability of achieving true *pCR*.

An explanation for the robustness and improved performance of our radiomics model is the use of ADC maps derived from DWI. We obtained 2252 features from the MRI data of each patient; after feature selection with a 2-sample *t*-test and LASSO logistic regression, 30 potential predictors were further analyzed. Only 1 pre-treatment T2WI feature was selected with LASSO for the construction of the radiomics signature, suggesting that T2WI was not a good option for *pCR* assessment after chemoradiotherapy. Several studies have shown the difficulty of identifying *pCR* using the morphological features exposed by T2WI (14,28,32). As such morphological features reflect only limited information about residual cancer cells post-chemoradiotherapy, DWI may provide more useful details. As a functional imaging technique, DWI showed strong potential in detecting subtle cancer cell remnants (29), and added valuable information regarding the responses to chemoradiotherapy in patients with LARC (15,30). The use of DWI may improve the performance and confidence of radiologists in selecting patients with *pCR* after chemoradiotherapy compared with conventional T2WI (14,15,28).

Another reason for the robustness of our model was the combination of pre- and post-treatment MRI data during analysis; this differed from what was done in a recent study (16). This combination is reflective of clinical practice and encompasses the entire diagnosis and treatment process. Most importantly, post-treatment MRI data represent the current status of the tumor after chemoradiotherapy; the data or information contained in post-treatment MRI scans correspond more closely to the surgical pathology. Hence, including post-treatment MRI data improves the model's reliability in detecting *pCR*. Our results showed that 19 of the 30 selected radiomic features were from post-treatment MRI data.

Moreover, the use of high-dimensional features also contributed to the performance of the model. Previous studies generally used low-dimensional information to evaluate the responses to chemoradiotherapy (23,28,29). However, in the present study, 90% (n=27) of the key features in the radiomics model were Gabor filtered wavelet features. Although the morphological and textural

features of tumors can easily be discerned, high-dimensional features are challenging to decipher with the naked eye (Figure S2), and ensuring that every clinician achieves a high level of expertise in gleaning detailed information from imaging features remains a significant obstacle. However, high-dimensional features hold more detailed information about the cancer and are more sensitive when assessing *pCR*, as was also demonstrated in a recent study (16). Hence, by incorporating these high-dimensional imaging features, a radiomics-based model can assist doctors in accurately identifying patients with *pCR* for whom a "wait and see" approach may be the most appropriate.

We used a nomogram as an individualized tool for *pCR* detection, and assessed whether the radiomics nomogram-based decisions could benefit patients. Decision curve analysis was applied to examine the clinical consequences based on threshold probability, from which a net benefit (defined as the proportion of true positives minus the proportion of false positives, weighted by the relative harm of false positive and false negative results) could be derived (26,33). The decision curve analysis proved that, given a threshold probability ranging from 0% to 100%, using the radiomics model to detect chemoradiotherapy outcomes provides a greater advantage than either the treat-all or treat-none scheme.

The use of the radiomics model not only provided an individualized tool for establishing a treatment plan, but also incorporated the radiomics signature and other clinical risk factors (age, sex, post-treatment CEA, post-treatment CA19-9, pre- and post-treatment tumor length, pre- and post-treatment TTOA, pre- and post-treatment IDBMP, pre- and post-treatment SDBMT, pre- and post-treatment NLN, and pre- and post-treatment MALLLN). The constructed radiomics model comprised of the radiomics signature and post-treatment tumor length. To the best of our knowledge, the post-treatment tumor length has never been proposed for *pCR* detection. Although its β value in the multivariate regression model was minuscule compared to that of the radiomics signature, post-treatment tumor length may provide complementary information for precise evaluation of *pCR* using the radiomics model. The potential association between post-treatment tumor length and *pCR* could be further investigated in future studies.

There were some limitations of the study. First, the sample size of patients with *pCR* was small relative to the entire cohort. Second, all the patients were from a single center. Although we categorized the patients into independent primary and validation cohorts according to their surgery dates, the model may perform differently if multicenter datasets with different parameters are used. A much larger dataset from multiple centers, with a considerably large sample of patients with *pCR*, ought to be investigated to validate the robustness and reproducibility of our proposed radiomics

model.

Conclusion

We propose a validated and easy-to-use radiomics model based on pre- and post-treatment MRI data for the individualized detection of *pCR* in patients with LARC. This model provides a noninvasive and convenient method to guide treatment planning in patients with LARC after they have undergone chemoradiotherapy.

This work was supported by the National Natural Science Foundation of China (Grant No. 81471640, 81501549, 81227901, 81501621 and 61231004), the Key Research Program of the Chinese Academy of Sciences (Grant No. KGZD-EW-T03), the Science and Technology Service Network Initiative of the Chinese Academy of Sciences (Grant No.KFJ-SW-STS-160) and the Beijing Municipal Science & Technology Commission 'Capital Clinical Research Special Fund' (No.Z171100001017102, Z151100004015105).

References

1. Kapiteijn E, Marijnen CA, Nagtegaal ID, Putter H, Steup WH, Wiggers T*, et al.* Preoperative radiotherapy combined with total mesorectal excision for resectable rectal cancer. The New England journal of medicine **2001**;345(9):638-46 doi 10.1056/NEJMoa010580.
2. van de Velde CJ, Boelens PG, Borras JM, Coebergh JW, Cervantes A, Blomqvist L*, et al.* EURECCA colorectal: multidisciplinary management: European consensus conference colon & rectum. European journal of cancer **2014**;50(1):1 e- e34 doi 10.1016/j.ejca.2013.06.048.
3. van Gijn W, Marijnen CA, Nagtegaal ID, Kranenbarg EM, Putter H, Wiggers T*, et al.* Preoperative radiotherapy combined with total mesorectal excision for resectable rectal cancer: 12-year follow-up of the multicentre, randomised controlled TME trial. The Lancet Oncology **2011**;12(6):575-82 doi 10.1016/S1470-2045(11)70097-3.
4. Sanghera P, Wong DW, McConkey CC, Geh JI, Hartley A. Chemoradiotherapy for rectal cancer: an updated analysis of factors affecting pathological response. Clinical oncology **2008**;20(2):176-83 doi 10.1016/j.clon.2007.11.013.
5. Maas M, Nelemans PJ, Valentini V, Das P, Rodel C, Kuo LJ*, et al.* Long-term outcome in patients with a pathological complete response after chemoradiation for rectal cancer: a pooled analysis of individual patient data. The Lancet Oncology **2010**;11(9):835-44 doi 10.1016/S1470-2045(10)70172-8.
6. Habr-Gama A, Perez RO, Proscurshim I, Campos FG, Nadalin W, Kiss D*, et al.* Patterns of failure and survival for nonoperative treatment of stage c0 distal rectal cancer following neoadjuvant chemoradiation therapy. J Gastrointest Surg **2006**;10(10):1319-28 doi 10.1016/j.gassur.2006.09.005.
7. Borschitz T, Wachtlin D, Mohler M, Schmidberger H, Junginger T. Neoadjuvant chemoradiation and local excision for T2-3 rectal cancer. Ann Surg Oncol **2008**;15(3):712-20 doi 10.1245/s10434-007-9732-x.
8. Maas M, Beets-Tan RGH, Lambregts DMJ, Lammering G, Nelemans PJ, Engelen SME*, et al.* Wait-and-See Policy for Clinical Complete Responders After Chemoradiation for Rectal Cancer. J Clin Oncol **2011**;29(35):4633-40 doi 10.1200/Jco.2011.37.7176.
9. Renehan AG, Malcomson L, Emsley R, Gollins S, Maw A, Myint AS*, et al.* Watch-and-wait approach versus surgical resection after chemoradiotherapy for patients with rectal cancer (the OnCoRe project): a propensity-score matched cohort analysis. Lancet Oncology **2016**;17(2):174-83 doi 10.1016/S1470-2045(15)00467-2.
10. Marijnen CAM. Organ preservation in rectal cancer: have all questions been answered? Lancet Oncology **2015**;16(1):E13-E22.
11. Janssen MHM, Ollers MC, Riedl RG, van den Bogaard J, Buijsen J, van Stiphout RGPM*, et al.* Accurate Prediction of Pathological Rectal Tumor Response after Two Weeks of Preoperative Radiochemotherapy Using (18)F-Fluorodeoxyglucose-Positron Emission Tomography-Computed Tomography Imaging. Int J Radiat Oncol **2010**;77(2):392-9 doi 10.1016/j.ijrobp.2009.04.030.
12. Engelen SME, Beets-Tan RGH, Lahaye MJ, Lammering G, Jansen RLH, van Dam RM*, et al.* MRI After Chemoradiotherapy of Rectal Cancer: A Useful Tool to Select Patients for Local Excision. Dis Colon Rectum **2010**;53(7):979-86 doi 10.1007/DCR.0b013e3181dc64dc.
13. Intven M, Reerink O, Philippens MEP. Dynamic contrast enhanced MR imaging for rectal cancer response assessment after neo-adjuvant chemoradiation. J Magn Reson Imaging **2015**;41(6):1646-53 doi 10.1002/jmri.24718.
14. Lambregts DMJ, Vandecaveye V, Barbaro B, Bakers FCH, Lambrecht M, Maas M*, et al.* Diffusion-Weighted MRI for Selection of Complete Responders After Chemoradiation for Locally Advanced Rectal Cancer: A Multicenter

Study. Ann Surg Oncol **2011**;18(8):2224-31 doi 10.1245/s10434-011-1607-5.

15. Blazic IM, Lilic GB, Gajic MM. Quantitative Assessment of Rectal Cancer Response to Neoadjuvant Combined Chemotherapy and Radiation Therapy: Comparison of Three Methods of Positioning Region of Interest for ADC Measurements at Diffusion-weighted MR Imaging. **2016**(1527-1315 (Electronic)).
16. Nie K, Shi L, Chen Q, Hu X, Jabbour SK, Yue NJ*, et al.* Rectal Cancer: Assessment of Neoadjuvant Chemo-Radiation Outcome Based on Radiomics of Multi-Parametric MRI. Clinical Cancer Research **2016**.
17. Lambin P, Rios-Velazquez E, Leijenaar R, Carvalho S, van Stiphout RGPM, Granton P*, et al.* Radiomics: Extracting more information from medical images using advanced feature analysis. European journal of cancer **2012**;48(4):441-6 doi 10.1016/j.ejca.2011.11.036.
18. Kumar V, Gu YH, Basu S, Berglund A, Eschrich SA, Schabath MB*, et al.* Radiomics: the process and the challenges. Magn Reson Imaging **2012**;30(9):1234-48 doi 10.1016/j.mri.2012.06.010.
19. Aerts HJWL, Velazquez ER, Leijenaar RTH, Parmar C, Grossmann P, Cavalho S*, et al.* Decoding tumour phenotype by noninvasive imaging using a quantitative radiomics approach. Nat Commun **2014**;5 doi Artn 4006 10.1038/Ncomms5006.
20. Gillies RJ, Kinahan PE, Hricak H. Radiomics: Images Are More than Pictures, They Are Data. Radiology **2016**;278(2):563-77 doi 10.1148/radiol.2015151169.
21. Itakura H, Achrol AS, Mitchell LA, Loya JJ, Liu T, Westbroek EM*, et al.* Magnetic resonance image features identify glioblastoma phenotypic subtypes with distinct molecular pathway activities. Sci Transl Med **2015**;7(303) doi ARTN 303ra138 10.1126/scitranslmed.aaa7582.
22. Altazi B, Fernandez D, Zhang G, Biagioli M, Moros E. Prediction of Cervical Cancer Treatment Response Using Radiomics Features Based On F18-FDG Uptake in PET Images. Med Phys **2015**;42(6):3326-.
23. Kickingereder P, Gotz M, Muschelli J, Wick A, Neuberger U, Shinohara RT*, et al.* Large-scale Radiomic Profiling of Recurrent Glioblastoma Identifies an Imaging Predictor for Stratifying Anti-Angiogenic Treatment Response. Clinical Cancer Research **2016**;22(23):5765-71 doi 10.1158/1078-0432.CCR-16-0702.
24. Huang YQ, Liang CH, He L, Tian J, Liang CS, Chen X*, et al.* Development and Validation of a Radiomics Nomogram for Preoperative Prediction of Lymph Node Metastasis in Colorectal Cancer. J Clin Oncol **2016**;34(18):2157-+ doi 10.1200/Jco.2015.65.9128.
25. Wang L, Li ZY, Li ZW, Li YH, Sun YS, Ji JF*, et al.* Efficacy and Safety of Neoadjuvant Intensity-Modulated Radiotherapy With Concurrent Capecitabine for Locally Advanced Rectal Cancer. Dis Colon Rectum **2015**;58(2):186-92 doi 10.1097/Dcr.0000000000000294.
26. Balachandran VP, Gonen M, Smith JJ, DeMatteo RP. Nomograms in oncology: more than meets the eye. Lancet Oncology **2015**;16(4):E173-E80.
27. Chang CC, Lin CJ. LIBSVM: A Library for Support Vector Machines. Acm T Intel Syst Tec **2011**;2(3) doi Artn 27 10.1145/1961189.1961199.
28. Curvo-Semedo L, Lambregts DMJ, Maas M, Thywissen T, Mehsen RT, Lammering G*, et al.* Rectal Cancer: Assessment of Complete Response to Preoperative Combined Radiation Therapy with Chemotherapy-Conventional MR Volumetry versus Diffusion-weighted MR Imaging. Radiology **2011**;260(3):734-43 doi 10.1148/radiol.11102467.
29. van der Paardt MP, Zagers MB, Beets-Tan RGH, Stoker J, Bipat S. Patients Who Undergo Preoperative Chemoradiotherapy for Locally Advanced Rectal Cancer Restaged by Using Diagnostic MR Imaging: A Systematic Review and Meta-Analysis. Radiology **2013**;269(1):101-12 doi 10.1148/radiol.13122833.
30. Kim SH, Lee JM, Hong SH, Kim GH, Lee JY, Han JK*, et al.* Locally advanced rectal cancer: added value of diffusion-weighted MR imaging in the evaluation of tumor response to neoadjuvant chemo- and radiation therapy. Radiology **2009**;253(1):116-25 doi 10.1148/radiol.2532090027.

31. Song I, Kim SH, Lee SJ, Choi JY, Kim MJ, Rhim H. Value of diffusion-weighted imaging in the detection of viable tumour after neoadjuvant chemoradiation therapy in patients with locally advanced rectal cancer: comparison with T2 weighted and PET/CT imaging. The British journal of radiology **2012**;85(1013):577-86 doi 10.1259/bjr/68424021.

32. Franklin JM, Anderson EM, Gleeson FV. MRI features of the complete histopathological response of locally advanced rectal cancer to neoadjuvant chemoradiotherapy. Clinical radiology **2012**;67(6):546-52 doi 10.1016/j.crad.2011.11.004.

33. Collins GS, Reitsma JB, Altman DG, Moons KGM, Grp T. Transparent Reporting of a Multivariable Prediction Model for Individual Prognosis or Diagnosis (TRIPOD): The TRIPOD Statement. Eur Urol **2015**;67(6):1142-51 doi 10.1016/j.eururo.2014.11.025.

Table 1. Characteristics of Patients in the Primary and Validation Cohorts

Characteristic	Primary cohort		P	Validation cohort		P
	pCR	*non-pCR*		*pCR*	*non-pCR*	
Age, mean ± SD, years	59.96±12.32	55.98±8.971	0.057	64.08±7.267	57.91±10.753	0.062
Gender (%)			0.371			0.764
Male	13(50%)	75(59.52%)		9(75%)	41(70.69%)	
Female	13(50%)	51(40.48%)		3(25%)	17(29.31%)	
Post-treatment CRT CEA (%)			***0.086***			***0.459***
Normal	26(100%)	108(85.71%)		12(100%)	51(87.93%)	
Abnormal	0(0%)	18(14.29%)		0(0%)	7(12.07%)	
Post-treatment CRT CA19-9 (%)			***0.971***			***1***
Normal	25(96.15%)	118(93.65%)		12(100%)	55(94.83%)	
Abnormal	1(3.85%)	8(6.35%)		0(0%)	3(5.17%)	
Histologic grade (%)			***0.381***			***0.167***
I	0(0%)	0(0%)		0(0%)	2(3.45%)	
II	22(84.62%)	113(89.68%)		8(66.67%)	48(82.76%)	
III	2(7.69%)	10(7.94%)		2(16.67%)	4(6.90%)	
IV	2(7.69%)	3(2.38%)		1(8.33%)	4(6.90%)	
V	0(0%)	0(0%)		1(8.33%)	0(0%)	
Pre-treatment T stage (%)			***0.287***			***1***
T0	0(0%)	0(0%)		0(0%)	0(0%)	
T1	0(0%)	0(0%)		0(0%)	0(0%)	
T2	6(23.08%)	15(11.90%)		2(16.67%)	8(13.80%)	
T3	19(73.08%)	96(76.19%)		10(83.33%)	45(77.59%)	
T4a	1(3.85%)	6(4.76%)		0(0%)	3(5.17%)	
T4b	0(0%)	9(7.14%)		0(0%)	2(3.45%)	
Pre-treatment N stage (%)			***0.299***			***0.439***
N0	2(7.69%)	9(7.14%)		1(8.33%)	2(3.45%)	
N1a	2(7.69%)	5(3.97%)		2(16.67%)	5(8.62%)	
N1b	5(19.23%)	28(22.22%)		1(8.83%)	5(8.62%)	
N2a	3(11.54%)	35(27.78%)		3(0.25%)	10(17.24%)	
N2b	14(53.85%)	49(38.89%)		5(41.67%)	36(62.07%)	
Post-treatment T stage (%)			<0.001*			<0.001*
T0	26(100%)	6(4.76%)		12(100%)	1(1.72%)	
T1	0(0%)	7(5.56%)		0(0%)	4(6.90%)	
T2	0(0%)	54(42.86%)		0(0%)	23(39.66%)	
T3	0(0%)	57(45.24%)		0(0%)	30(51.72%)	
T4a	0(0%)	1(0.79%)		0(0%)	0(0%)	

T4b	0(0%)	1(0.79%)		0(0%)	0(0%)	
Post-treatment N stage (%)			***0.020****			***0.295***
N0	26(100%)	86(68.25%)		12(100%)	37(63.80%)	
N1a	0(0%)	23(18.25%)		0(0%)	7(12.07%)	
N1b	0(0%)	11(8.73%)		0(0%)	8(13.79%)	
N2a	0(0%)	3(2.38%)		0(0%)	5(8.62%)	
N2b	0(0%)	3(2.38%)		0(0%)	1(1.72%)	
Pre-treatment TL	41.38±15.118	45.94±13.784	0.133	41.83±12.372	45.53±13.507	0.384
Pre-treatment TTOA	14.27±4.006	15.77±5.141	0.163	15.50±4.275	17.28±5.486	0.295
Pre-treatment IDBMP	2.65±2.497	5.27±4.384	<0.01*	4.67±7.215	6.17±6.344	0.467
Pre-treatment SDBMT	5.85±5.951	4.04±3.844	0.051	3.75±2.768	4.66±5.857	0.604
Pre-treatment NLN	12.38±5.838	12.45±5.790	0.957	10.00±4.880	12.53±4.946	0.110
Pre-treatment MALLLN	5.88±3.548	6.59±3.371	0.339	4.83±1.642	7.16±3.583	0.032*
Post-treatment TL	27.42±9.892	29.89±10.211	0.262	22.25±6.440	27.33±9.267	0.076
Post-treatment TTOA	8.50±2.997	9.71±3.237	0.08	6.75±2.006	9.71±3.195	<0.01*
Post-treatment IDBMP	0.85±1.541	2.37±3.209	0.019*	1.50±1.977	2.74±3.832	0.280
Post-treatment SDBMT	7.62±5.224	5.35±4.670	0.029*	7.33±4.141	6.88±6.644	0.821
Post-treatment NLN	7.23±3.840	7.69±3.914	0.585	5.67±2.871	7.19±3.390	0.152
Post-treatment MALLLN	3.54±1.702	4.40±3.124	0.177	2.92±1.443	4.26±2.475	0.075
Radiomics Score (mean ± SD)	0.7017±0.2687	0.0995±0.1128	<0.01*	0.6957±0.2756	0.0815±0.1041	<0.01*

Note: ***Chi-Square or Fisher Exact tests, as appropriate, were used to compare the differences in categorical variables*** (Gender, Post-treatment CEA, Post-treatment CA19-9, Histologic grade, Pre- and Post-treatment T stage, and Pre- and Post-treatment N stage), while a two-sample t-test was used to compare the differences in age, Radiomics Score, Pre- and Post-treatment TL, Pre- and Post-treatment TTOA, Pre- and Post-treatment IDBMP, Pre- and Post-treatment SDBMT, Pre- and Post-treatment NLN and Pre- and Post-treatment MALLLN. Laboratory analysis of CEA and CA 19-9 were done via routine blood tests within 1 week before surgery. The threshold value for CEA level was ≤5 ng/mL and > 5 ng/mL and the threshold value for CA 19-9 level was ≤39 U/mL and > 39 U/mL, according to the normal range used in clinics.

Abbreviations: *pCR*, pathological complete response; CEA, carcinoembryonic antigen; CA19-9, carbohydrate antigen 19-9; SD, standard deviation; ADC, apparent diffusion coefficient. Tumor's length, TL; Tumor's thickness obtained from oblique axial T2WI, TTOA; The invasion distance beyond the muscularis propria, IDBMP; The shortest distance between the mesorectal fascia and the outer edge of the tumor extension, SDBMT; Total number of the lymph nodes detected by DWI, NLN; The minor axis length of the largest lymph node, MALLLN.

* $P < 0.05$

Table 2. Performance of the radiomics signature and radiomics model

Metrics	Radiomics Signature		Radiomics Model	
	Primary cohort	Validation cohort	Primary cohort	Validation cohort
Accuracy (95%)	94.08% (93.19% to 94.79%)	94.29% (94.21% to 95.61%)	96.05% (94.67%, 97.59%)	94.29% (91.85%, 97.11%)
AUC (95%)	0.9744 (0.9642 to 0.9756)	0.9799 (0.9780 to 0.9840)	0.9799 (0.9517 to 1)	0.9756 (0.9417 to 1)
PPV (95%)	86.96% (84.84% to 90.40%)	90.00% (89.60% to 99.40%)	91.67% (86.56%, 97.06%)	90.00% (79.51%, 99.12%)
NPV (95%)	95.35% (94.39% to 95.81%)	95.00% (94.87% to 95.17%)	96.88% (95.42%, 98.34%)	95.00% (92.19%, 97.65%)

Abbreviations: AUC, area under ROC curve; PPV, Positive Predictive Value; NPV, Negative Predictive Value

Figure Legends

Figure 1. Flowchart of the study.

With manually segmented tumor masks, we first extracted 2252 quantitative radiomic features from masked pre- and post-treatment T2 weighted imaging and diffusion-weighted imaging data; the general view of the feature extraction algorithm is shown. Next, 2 feature selection steps were applied on the extracted features with a 2- sample *t*-test and the least absolute shrinkage and selection operator (LASSO). Thereafter, a radiomics signature was constructed with the selected features using the linear kernel support vector machine model. Finally, the radiomics signature and clinical factors were incorporated into a nomogram for individual evaluation. ROC, receiver operating characteristic.

Figure 2. **Tuning parameter selection for feature selection (λ) and support vector machine model construction (C).**

(A) Feature selection with least absolute shrinkage and selection operator using leave-one-out cross-validation (LOOCV) via minimum criteria. The misclassification error was plotted versus log (λ). A dotted vertical line was drawn at the optimal value by using the minimum criteria. A λ value of 0.014189 was chosen according to the LOOCV. (B) The optimal value regularization parameter C selection for the SVM model construction using LOOCV. The area under the receiver operating characteristic curve (AUC) was plotted *vs.* C. A dotted vertical line was drawn at the optimal value. The C value of 0.05 was chosen according to the LOOCV.

Figure 3. **Radiomic features and performance of the radiomics signature.**

(A) Heat map of 30 selected radiomic features. Each row corresponds to 1 radiomic feature, and each column corresponds to 1 patient (separately grouped for the primary vs. validation cohort and the pathological complete response [*pCR*] *vs. non-pCR* group). (B) The radiomics score for each patient and receiver operating characteristic (ROC) curve in the primary cohort. (C) The radiomics score for each patient and ROC curve in the validation cohort.

Figure 4. **Nomogram developed with the radiomics model and calibration curves, as well as the decision curve derived from the radiomics model.**

(A) The developed radiomics nomogram. (B) Calibration curves of the radiomics model in the primary and validation cohorts. Calibration curves depict the calibration of each model in terms of the agreement between the predicted probability of pathological complete response (*pCR*) and actual outcomes of the *pCR* rate. The y-axis represents the actual rate of *pCR*. The x-axis represents the predicted probability of *pCR*. The diagonal blue line represents a perfect prediction by an ideal

model. The pink line represents the performance of the radiomics model, of which a closer fit to the diagonal blue line represents a better prediction. (C) Decision curve analysis for the radiomics model. The y-axis measures the net benefit. The pink line represents the radiomics model. The blue line represents the assumption that all patients showed *pCR*. The black line represents the assumption that no patients showed *pCR*.

Figure 1

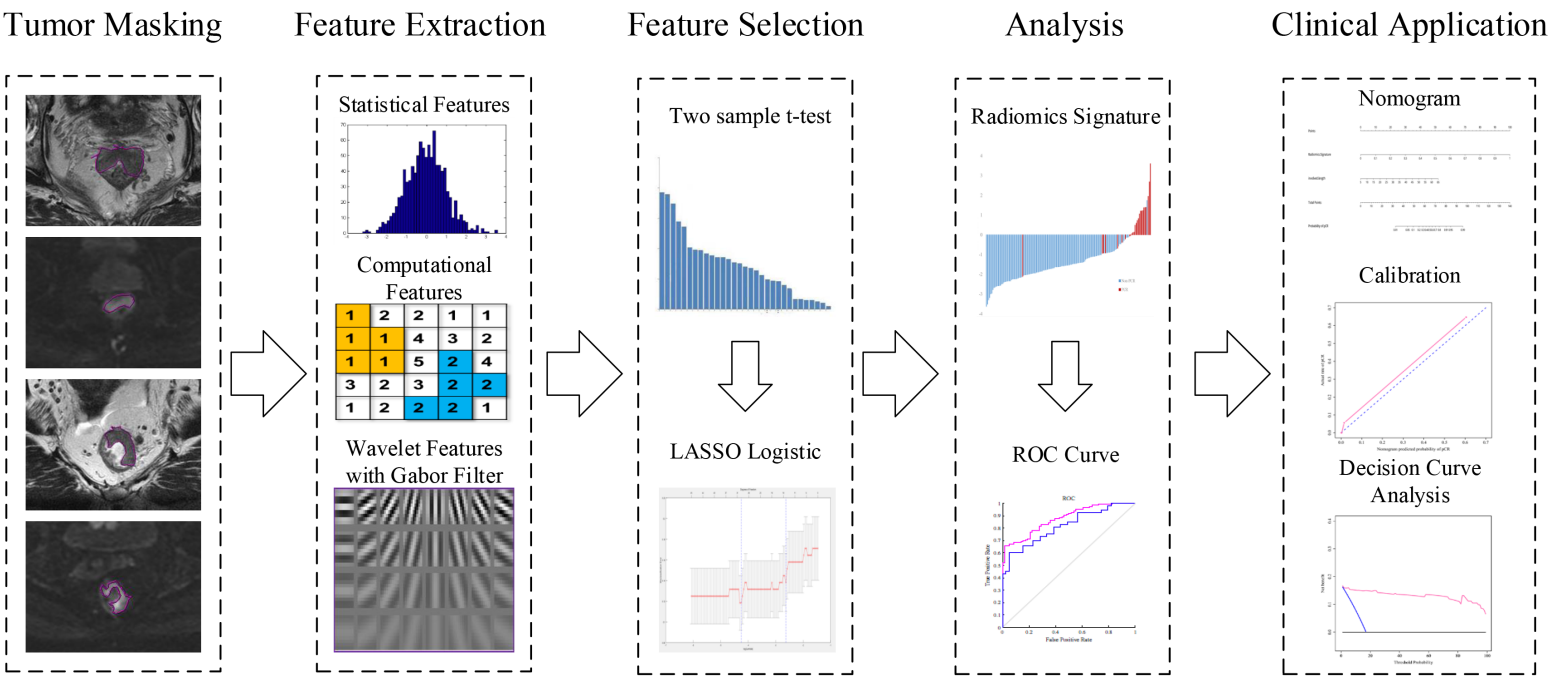

Figure 2

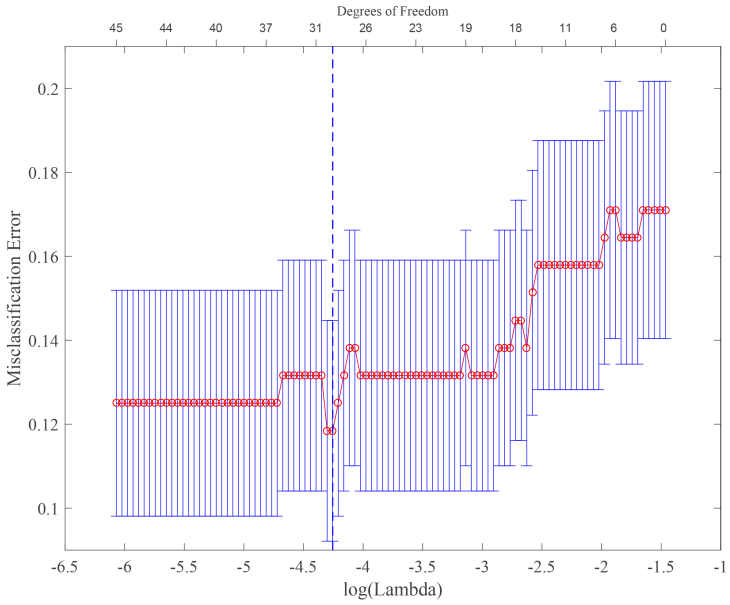

A

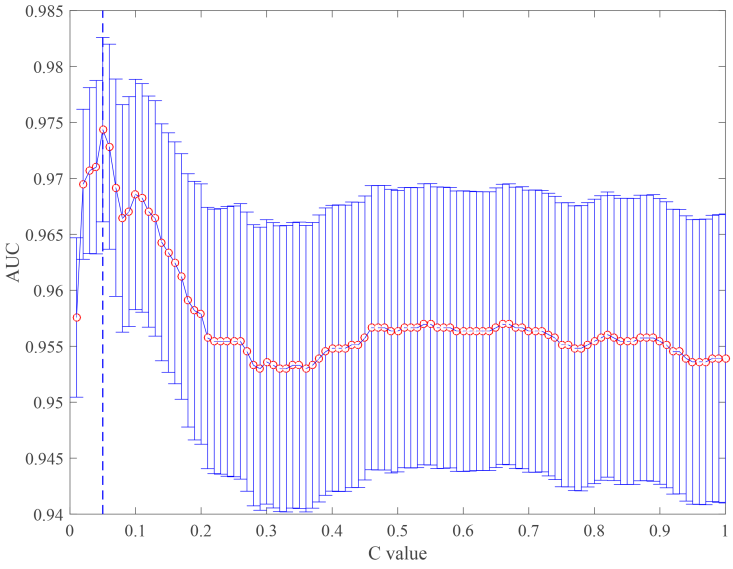

B

Figure 3

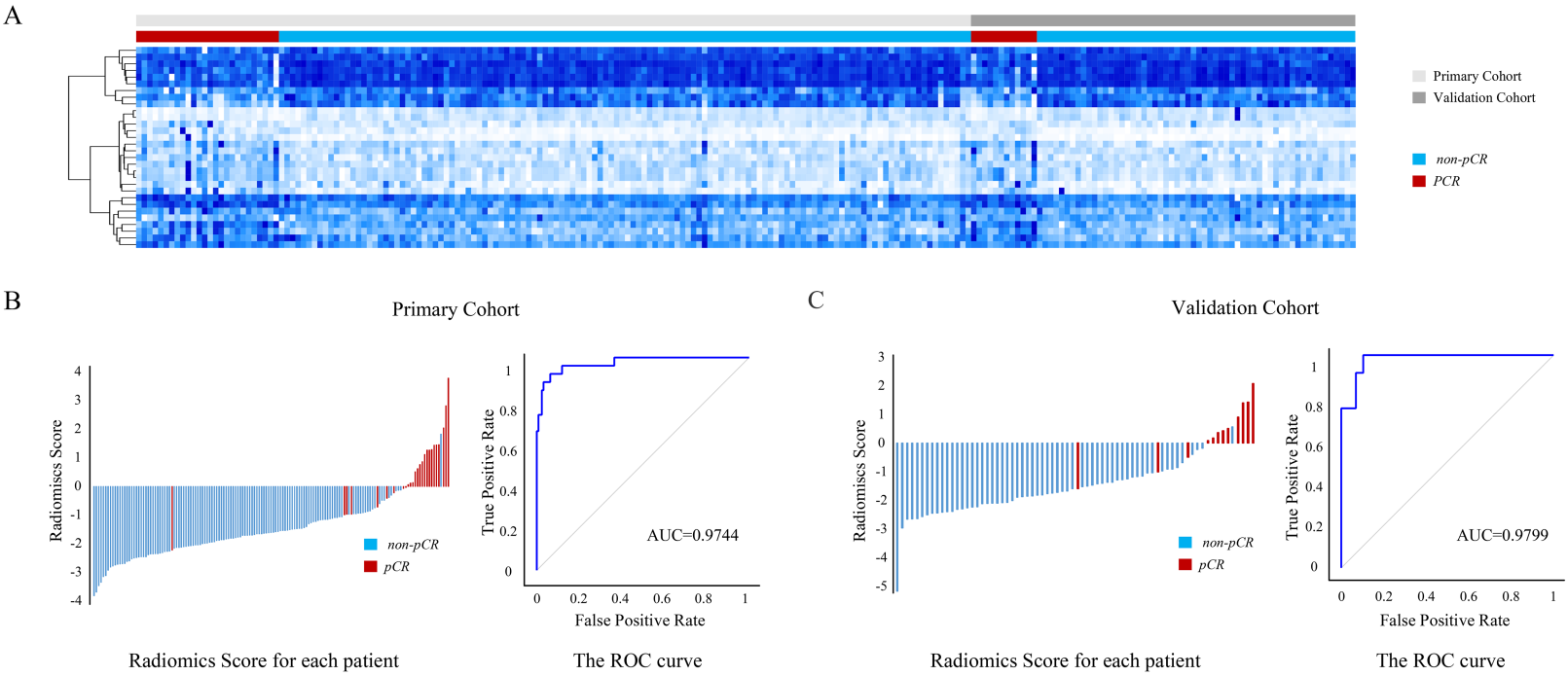

Figure 4

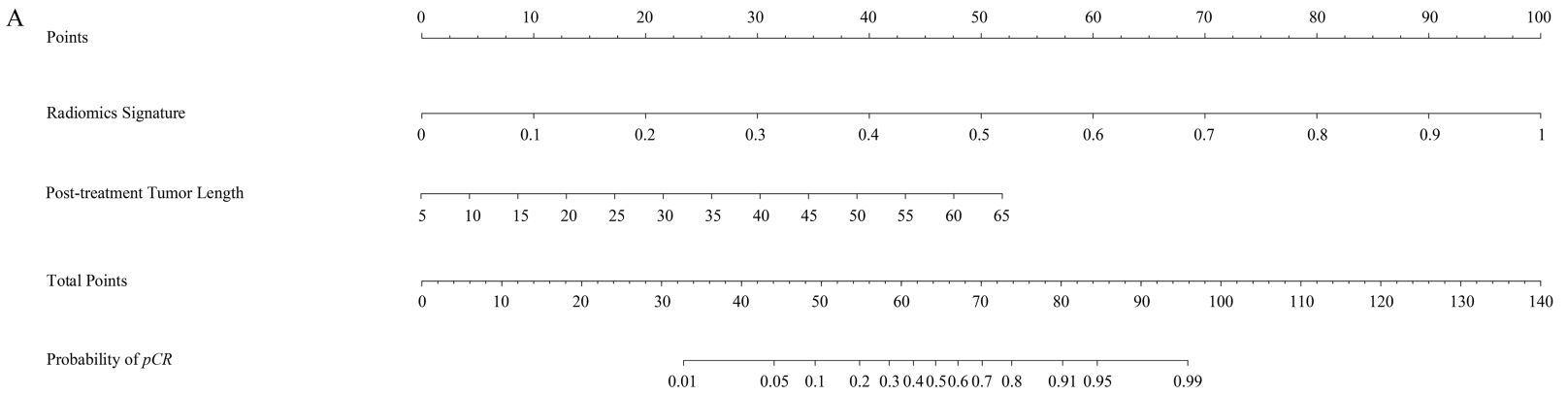

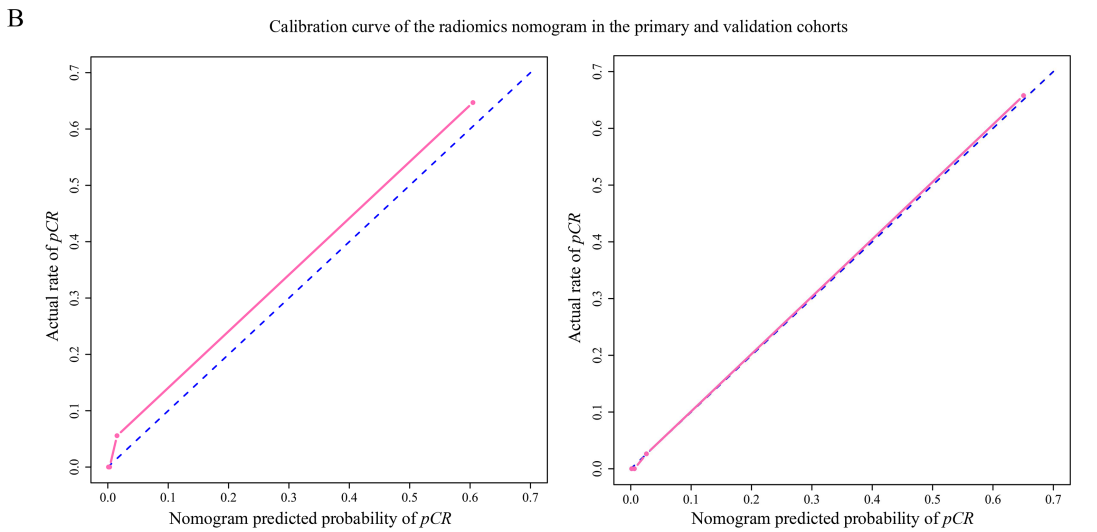

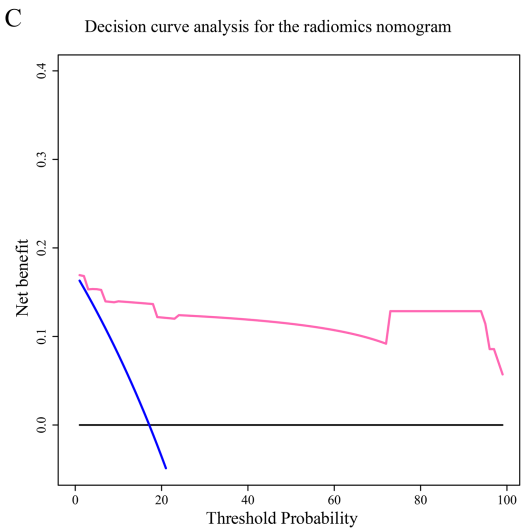

AACR American Association for Cancer Research

Clinical Cancer Research

Radiomics Analysis for Evaluation of Pathological Complete Response to Neoadjuvant Chemoradiotherapy in Locally Advanced Rectal Cancer

Zhenyu Liu, Xiao-Yan Zhang, Yan-Jie Shi, et al.

Clin Cancer Res Published OnlineFirst September 22, 2017.